Solid State Communications 149 (2009) 126–130

Contents lists available at ScienceDirect

Solid State Communications

journal homepage: www.elsevier.com/locate/ssc

Magnetic polaron structures in the one-dimensional double and super-exchange model

E. Vallejo [a,*], F. López-Urías [b], O. Navarro [a], M. Avignon [c]

[a] Instituto de Investigaciones en Materiales, Universidad Nacional Autónoma de México, Apartado Postal 70-360, 04510 México D. F., Mexico
[b] Advanced Materials Department, IPICYT, Camino a la Presa San José 2055, Lomas 4a sección, 78216, San Luis Potosí, San Luis Potosí, Mexico
[c] Institut Néel, Centre National de la Recherche Scientifique (CNRS) and Université Joseph Fourier, BP 166, 38042 Grenoble Cedex 9, France

ARTICLE INFO

Article history:
Received 5 September 2008
Received in revised form
29 October 2008
Accepted 4 November 2008 by C. Lacroix
Available online 11 November 2008

PACS:
75.30.Et
75.10.Hk
64.75.+g

Keywords:
D. Exchange and super-exchange interactions
D. Classical spin models
D. Phase separation

ABSTRACT

An analytical and numerical study of the one-dimensional double and super-exchange model is presented. A phase separation between ferromagnetic and anti-ferromagnetic phases occurs at low super-exchange interaction energy. When the super-exchange interaction energy gets larger, the conduction electrons are self-trapped within separate small magnetic polarons. These magnetic polarons contain a single electron inside two or three sites depending on the conduction electron density and form a Wigner crystallization. A new phase separation is found between these small polarons and the anti-ferromagnetic phase. Our results could explain the spin-glass-like behavior observed in the nickelate one-dimensional compound $Y_{2-x}Ca_xBaNiO_5$.

© 2008 Elsevier Ltd. All rights reserved.

1. Introduction

Magnetic ordering of localized spins mediated by nonmagnetic conduction electrons, the so-called double exchange (DE) or indirect exchange, is the source of a variety of magnetic behavior in transition metal and rare-earth compounds [1]. Conversely, this interplay affects the mobility of the carriers and may lead to interesting transport properties such as colossal magnetoresistance in manganites. The origin of the DE lies in the intra-atomic coupling of the spin of the itinerant electrons with localized spins $\vec{S}_i$. In this coupling, localized and itinerant electrons belong to the same atomic shell. According to Hund's rule, the coupling is ferromagnetic (F) when the local spins have less than half-filled shells and anti-ferromagnetic (AF) for more than half-filled shells [2]. This mechanism has been widely used in the context of manganites [2–4]. A similar coupling also occurs in Kondo systems via the so-called s–d exchange model. In this case, local spins are from a d shell (or f shell in rare-earth compounds) while the conduction electrons are from s or p states and the coupling is anti-ferromagnetic. In recent literature the ferromagnetic coupling case is often referred to as the Ferromagnetic Kondo model. Independently of the sign of the coupling, the "kinetic" energy lowering, favors a F background of local spins. This F tendency is expected to be thwarted by AF super-exchange (SE) interactions between localized spins $\vec{S}_i$ as first discussed by de Gennes [5] who conjectured the existence of canted states. In spite of recent interesting advances, our knowledge of magnetic ordering resulting from this competition is still incomplete.

Although it may look academic, the one-dimensional (1D) version of this model is very illustrative and helpful in building an unifying picture. On the other hand, the number of pertinent real 1D systems as the nickelate one-dimensional metal oxide carrier-doped compound $Y_{2-x}Ca_xBaNiO_5$ [6] is increasing. In this compound, carriers are essentially constrained to move parallel with NiO chains and a spin-glass-like behavior was found at very low temperatures $T \lesssim 3$ K for typical dopings $x = 0.045$, 0.095 and 0.149. Recently, it has been shown that three-leg ladders in the oxyborate system Fe_3BO_5 may provide evidence for the existence of spin and charge ordering resulting from such a competition [7].

Naturally, the strength of the magnetic interactions depends significantly on the conduction band filling, x. At low conduction electron density, F polarons have been found for localized $S = 1/2$ quantum spins [8]. "Island" phases, periodic arrangement

* Corresponding author.
E-mail address: emapion@yahoo.com (E. Vallejo).

0038-1098/$ – see front matter © 2008 Elsevier Ltd. All rights reserved.
doi:10.1016/j.ssc.2008.11.001

of F polarons coupled anti-ferromagnetically, have been clearly identified at commensurate fillings both for quantum spins in one dimension [9] and for classical spins in one [10] and two dimensions [11]. Phase separation between hole-undoped antiferromagnetic and hole-rich ferromagnetic domains has been obtained in the Ferromagnetic Kondo model [12]. Phase separation and small ferromagnetic polarons have been also identified for localized $S = 3/2$ quantum spins [13]. Therefore, it is of importance to clarify the size of the polarons, and whether it is preferable to have island phases, separate small polarons or eventually large polarons.

In this paper, we present an analytical and numerical study of the one-dimensional double and super-exchange model. Our results provide a plausible understanding of the ground state of the nickelate 1D compound $Y_{2-x}Ca_xBaNiO_5$ allowing a straightforward explanation of its spin-glass-like behavior [6]. The paper is organized as follows. In Section 2 a brief description of the model is given. In Section 3, results and a discussion are presented. Finally, our results are summarized in Section 4.

2. The model

The DE Hamiltonian is originally of the form,

$$H = -\sum_{i,j;\sigma} t_{ij}(c^+_{i\sigma}c_{j\sigma} + h.c.) - J_H \sum_i \vec{S}_i \cdot \vec{\sigma}_i, \quad (1)$$

where $c^+_{i\sigma}(c_{i\sigma})$ are the fermions creation (annihilation) operators of the conduction electrons at site i, t_{ij} is the hopping parameter and $\vec{\sigma}_i$ is the electronic conduction band spin operator. In the second term, J_H is the Hund's exchange coupling. Here, Hund's exchange coupling is an intra-atomic exchange coupling between the spin of conduction electrons $\vec{\sigma}_i$ and the spin of localized electrons $\vec{S}_i$. This Hamiltonian simplifies in the strong coupling limit $J_H \to \infty$, a limit commonly called itself the DE model. We will consider the local spins as classical $\vec{S}_i \to \infty$, a reasonable approximation in many cases in view of the similarity of the known results [9,12]. The DE Hamiltonian takes the well-known form,

$$H = -\sum_{i,j} t_{i,j} \cos\left(\frac{\theta_{i,j}}{2}\right)(c^+_i c_j + h.c.). \quad (2)$$

The itinerant electrons being now either parallel or antiparallel with the local spins are thus spinless. $\theta_{i,j}$ is the relative angle between the classical localized spins at sites i and j which are specified by their polar angles ϕ_i, φ_i defined with respect to a z-axis taken as the spin quantization axis of the itinerant electrons. The super-exchange coupling is an anti-ferromagnetic inter-atomic exchange coupling between localized spins $\vec{S}_i$. The complete one-dimensional DE + SE Hamiltonian becomes,

$$H = -t\sum_i \cos\left(\frac{\theta_i}{2}\right)(c^+_i c_{i+1} + h.c.) + J\sum_i \vec{S}_i \cdot \vec{S}_{i+1}, \quad (3)$$

where $\theta_{i,i+1} = \theta_i$ and J is the super-exchange interaction energy.

3. Results and discussion

In this section, we determine the complete phase diagram in one dimension as a function of the super-exchange interaction energy J and the conduction electron density x, showing that up to now the model has not revealed all its richness. Besides the quantum results already published [8,9,13] we find two types of phase separation. In addition to the expected F–AF phase separation appearing for small J, we obtain a new phase separation

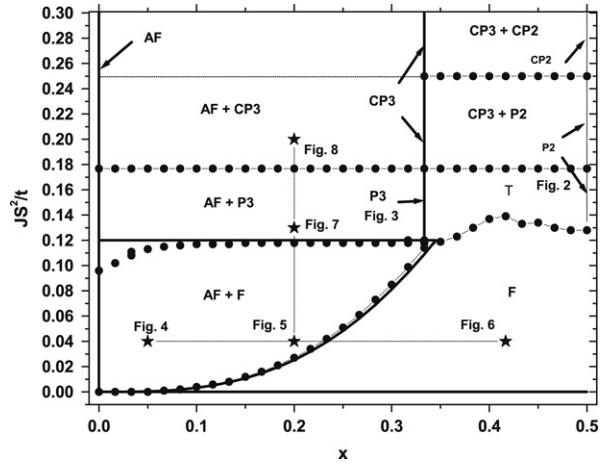

Fig. 1. Magnetic phase diagram as a function of the SE energy J and the conduction electron density x. A dotted line in this diagram represents a guide for the eyes. The different phases are described in the text.

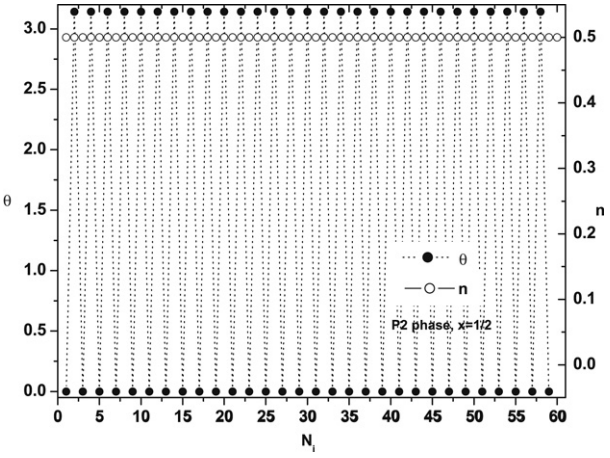

Fig. 2. P2 phase for $x = 1/2$, showing $N-1$ angles (θ) and charge distribution (n). Angles in this figure are 0 or π exactly.

between small polarons (one electron within two or three sites) and AF regions for larger J. It is interesting to note that large polarons are never found stable in this limit.

The magnetic phase diagram has been obtained at $T = 0$ K by using open boundary conditions on a linear chain of $N = 60$ sites. For a given conduction electron density x ($0 \le x \le 0.5$ because of the hole–electron symmetry), we have to optimize all the $N-1$ angles θ_i. For this goal, we use an analytical optimization and a classical Monte Carlo method. The analytical solution has been tested as a starting point in the Monte Carlo simulation.

Our results are summarized in Fig. 1, showing the whole magnetic phase diagram.

For the commensurate fillings $x = 1/2$ and $1/3$, we recover the "island" phases with ferromagnetic polarons ($\theta_i = 0$) separated by antiferromagnetic links ($\theta_i = \pi$), P2 ($\cdots \uparrow\uparrow\downarrow\downarrow\uparrow\uparrow\downarrow\downarrow\uparrow\uparrow\downarrow\downarrow \cdots$) and P3 ($\cdots \uparrow\uparrow\uparrow\downarrow\downarrow\downarrow\uparrow\uparrow\uparrow\downarrow\downarrow\downarrow \cdots$), Figs. 2 and 3 respectively, identified previously for classical [10] and $S = 1/2$ quantum [9] local spins. In the quantum case, the real space spin–spin correlations illustrate such structures. For these phases, the analytical optimization implies angles 0 or π exactly.

The electrons are individually self-trapped in small independent ferromagnetic polarons of two and three sites respectively forming a Wigner crystallization. In reference [14], a spiral phase has been proposed instead of the P2 phase for $x = 1/2$. The ferromagnetic phase is stable for weak SE interaction below P2 phase, P2 phase becomes stable for $\frac{2}{\pi} - \frac{1}{2} < JS^2/t < \frac{1}{4}$. For $JS^2/t > \frac{1}{4}$, P2

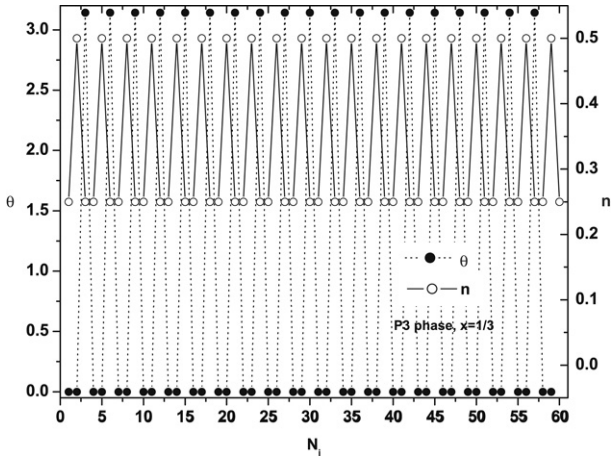

Fig. 3. P3 phase for $x = 1/3$, showing the same as in Fig. 2.

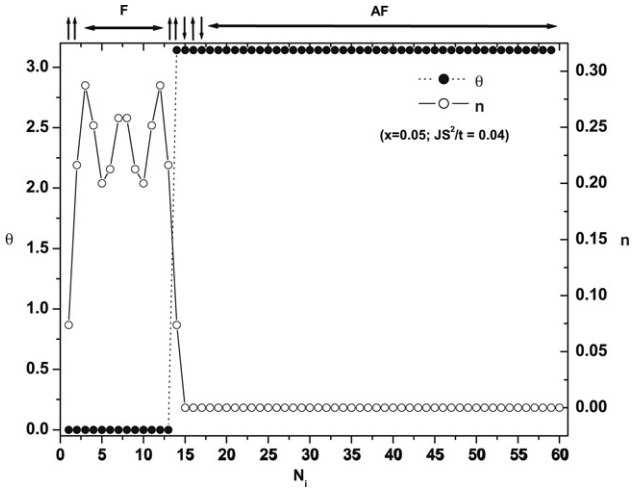

Fig. 4. AF + F phase at $x = 0.05$ (3 electrons) and $JS^2/t = 0.04$, showing $N - 1$ angles, charge distribution and a spin configuration snapshot.

transforms into a canted polaron phase CP2 in which the angle inside the F islands becomes finite (θ_1) while the angle between the polarons (θ_2) still keeps the value π. A complete analytical solution can be derived in this case.

Similar phases P3 and CP3 are obtained for $x = 1/3$. In CP3, two angles θ_1, θ_2 are finite inside the 3-site polaron while, between polarons, $\theta_3 = \pi$. This phase has a general continuous degeneracy within each 3-site polaron given by the condition,

$$\cos(\theta_1) + \cos(\theta_2) = \frac{1}{8(JS^2/t)^2} - 2. \tag{4}$$

An example of this degeneracy of the spin configuration is clearly seen in Fig. 8 where different sets of angles (θ_1, θ_2) appear within the CP3 phase. Both CP2 and CP3 evolve towards complete anti-ferromagnetism as $JS^2/t \to \infty$, see Eq. (4). P3 $\to$ CP3 at $\frac{JS^2}{t} = \frac{1}{4\sqrt{2}}$. These phases result from the "spin-induced Peierls $2k_F$ instability" due to the modulation of the hopping with $I = 1/x$ angles. For lower commensurate fillings $x < 1/3$, such P_l polaron phases are not found stable. Instead, next to the F phase at low J we find AF–F phase separation. Of course, an anti-ferromagnetic phase always occurs at $x = 0$. Fig. 1 shows that when the SE interaction energy is small $JS^2/t \lesssim 0.12$, the F phase occurs for a large conduction electron density. The F–AF transition is given by the F–AF phase separation (AF + F in Fig. 1) consisting of one large ferromagnetic polaron within an AF background as can be seen in Figs. 4 and 5, for a typical value of $JS^2/t = 0.04$. All electrons are inside the polaron. The position of the polaron within the linear chain is not important because of translation degeneracy. These figures also show charge distribution (n) inside each polaron and a spin configuration snapshot. In this region, the polarons' size diminishes with the conduction electron density, (Figs. 4 and 5). For this F–AF phase separation, the analytical optimization implies angles 0 and π exactly for the F and AF domains respectively (Figs. 4 and 5). In the thermodynamic limit $N \to \infty$, and for $M \gg 3$ sites (M being the size of the F domain), the energy is obtained as,

$$\frac{U}{Nt} = -2x\cos(x_o\pi) - \frac{JS^2}{t}, \tag{5}$$

for $x \leq x_o$. x_o corresponds to the Maxwell construction between the anti-ferromagnetic energy $\frac{U}{Nt} = -\frac{JS^2}{t}$ and the ferromagnetic one $\frac{U}{Nt} = -\frac{2}{\pi}\sin(x\pi) + \frac{JS^2}{t}$. x_o is given by the following equation,

$$x_o\cos(x_o\pi) - \frac{1}{\pi}\sin(x_o\pi) + \frac{JS^2}{t} = 0. \tag{6}$$

The corresponding boundary given by Eq. (6) is shown by the full line in Fig. 1. The analytical results for $N = 60$ sites are very close to this line. When the conduction electron density gets larger $x \geq x_o$, the F–AF phase separation becomes the F phase. The size of the ferromagnetic polaron in the thermodynamic limit ($N \to \infty, M \gg 3$) is $\epsilon = \frac{M}{N} = \frac{x}{x_o}$, for $x \leq x_o$, and $\epsilon = 1$ in the ferromagnetic phase. An important effect of lattice distortion is expected between these F and AF domains [7]. The effect of lattice distortion can be studied in the F–AF phase separation using the following density matrix elements. Inside the F domain the matrix elements are given by,

$$\rho_{i,j} = \frac{2}{M+1}\sum_{p=1}^{xN}\left(\sin\frac{(p)(i)\pi}{M+1}\right)\left(\sin\frac{(p)(j)\pi}{M+1}\right). \tag{7}$$

Between F–AF domains and within AF domains the matrix elements are zero. These density matrix elements suggest an important lattice distortion inside F domains and null between F–AF domains and within AF domains. This lattice distortion could be detectable for example using neutron diffraction techniques as in $La_2CuO_{4+\delta}$ [12]. Charge distribution is easily obtained for $n_i = \rho_{i,j=i}$ (Figs. 2–7). For example in Fig. 6, charge distribution of the F phase can be observed for 25 electrons and at $\frac{JS^2}{t} = 0.04$. For small SE interaction, the F–AF phase separation has been reported in two dimensions [15], in one dimension using classical localized spins and $J_H = 8$ [14] and in the one-dimensional ferromagnetic Kondo model [16]. Quantum results for $S = 3/2$, showed phase separation when Coulomb repulsion was taken into account [13]. We can see that in this limit, our results differ from those of Koshibae et al. [10] within the "spin-induced Peierls instability" mechanism.

At low concentration $x < 1/3$, if the SE interaction energy increases $0.12 \lesssim JS^2/t \lesssim \frac{1}{4\sqrt{2}}$, we find a new phase separation between P3 and AF phases as shown in Figs. 1 and 7. It transforms into AF + CP3 for $JS^2/t > \frac{1}{4\sqrt{2}}$ as P3 becomes CP3. A phase such as AF + P3(CP3) has been identified using $S = 3/2$ quantum spins [13]. Figs. 7 and 8 show the AF + P3 and the AF + CP3 phases with 12 electrons among the 60 sites for typical values of the SE interaction energy $JS^2/t = 0.13$ and $JS^2/t = 0.20$ respectively. These phase separations consisting in P3 or CP3 phases in an AF background and they are degenerate with phases where the polarons can be ordered or not, while keeping the number of F and AF bonds fixed. The phase obtained within the "spin-induced Peierls instability" [10] belongs to this class. The former degeneracy unifies ideas like phase separation and individual polarons and gives a natural response to the instability

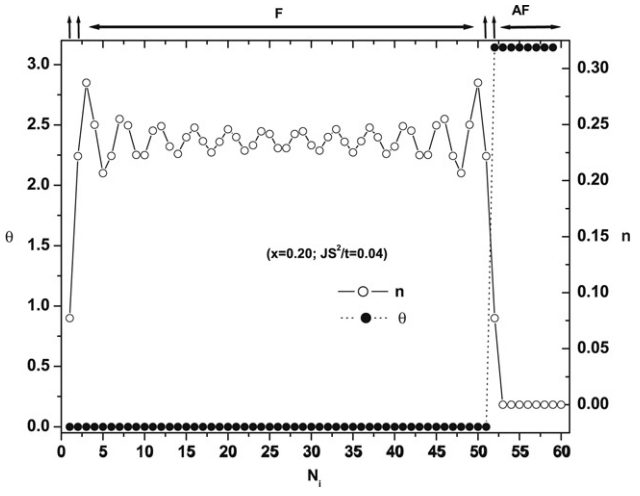

Fig. 5. The same as in Fig. 4, but at $x = 0.20$ (12 electrons).

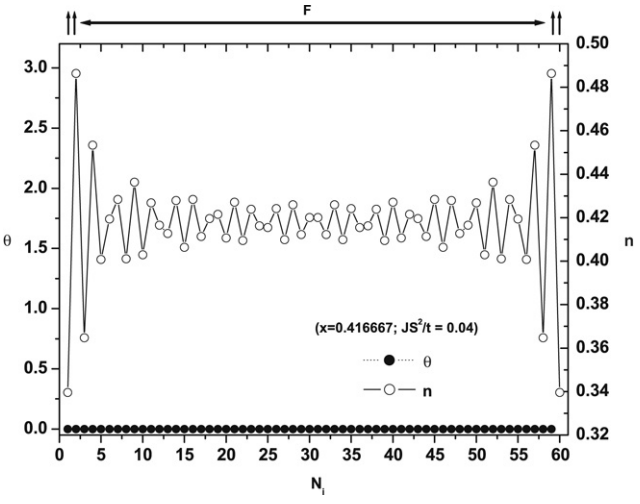

Fig. 6. F phase at $x = \frac{25}{60}$ (25 electrons) and $JS^2/t = 0.04$, showing the same as in Fig. 4.

at the Fermi energy and to an infinite compressibility as well. In the thermodynamic limit, P3–AF phase separation energy is given by the following equation

$$\frac{U}{Nt} = \left(-\sqrt{2} + 4\frac{JS^2}{t}\right)x - \frac{JS^2}{t}. \tag{8}$$

We find that the AF+F → AF+P3 transition is first order. In Fig. 1, the transition line $JS^2/t \simeq 0.12$ between the two phase separations AF + P3 and AF + F has been determined using the corresponding energies in the thermodynamic limit. Density matrix elements suggest a large lattice distortion within each 3-site polaron in P3 phase. Charge distribution among the 3 sites $i = 1, 2, 3$ inside each polaron is $n_1 = n_3 = \frac{1}{4}$ and $n_2 = \frac{1}{2}$, see Fig. 7.

Phase separation also takes place for fillings between $x = 1/2$ and $x = 1/3$ for SE interactions $JS^2/t \geq \frac{1}{4\sqrt{2}}$. It is between CP3 and P2 or CP2 due to the canting inside the P2 polaron with increasing J. The transition between the two occurs for $JS^2/t = 0.25$, where $P2 \rightarrow CP2$. Again, due to the AF links between the polarons these phase separations are degenerate with respect to the position of the two types of polarons. Below CP3 + P2, the phase labeled T in Fig. 1 is a more general complex phase obtained by the Monte Carlo method and can be polaronic like or not. Close to the boundary with CP3 + P2 this phase resembles the P3 + P2 phase separation, so as seen in Fig. 1, the transition line

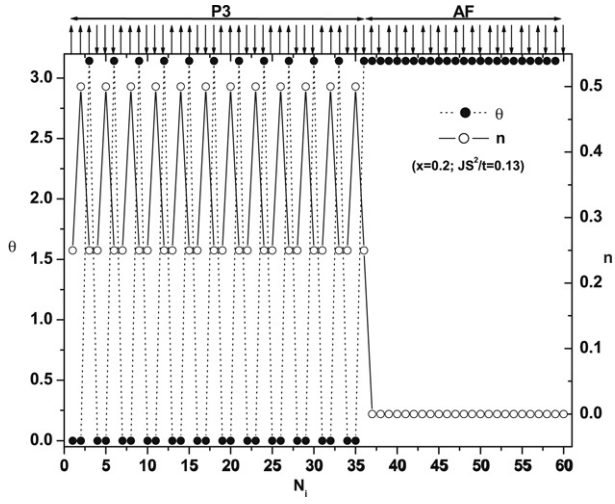

Fig. 7. AF + P3 phase at $x = 0.20$ (12 electrons) and $JS^2/t = 0.13$, showing $N - 1$ angles, charge distribution and a spin configuration snapshot.

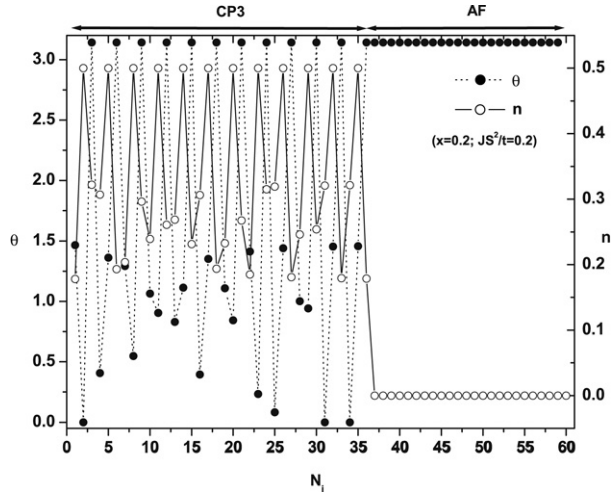

Fig. 8. AF + CP3 phase at $x = 0.20$ (12 electrons) and $JS^2/t = 0.20$, showing the same as in Fig. 7.

$JS^2/t = \frac{1}{4\sqrt{2}}$, corresponding to P3 → CP3, is second order. This boundary also extends in the region $x < 1/3$ between AF + P3 and AF + CP3. For the SE interaction region $JS^2/t > \frac{1}{4}$ ($JS^2/t = \frac{1}{4}$ is shown by the short-dotted line in Fig. 1), the spin configurations (θ_1, π) or (π, θ_2), i.e a CP2 polaron plus an AF link, belong to all the possible degenerate configurations of CP3 polarons as can be seen from Eq. (4). This means that in this region phase separation AF + CP3 may also contain a number of two-sites canted polarons CP2. Similarly, this also occurs within CP3 + CP2 phase. The total number of polarons remaining equal to the number of electrons; we can label it as AF + CP3 + CP2. A single energy is found in the whole conduction electron density regime ($0 \leq x \leq 0.5$). In the thermodynamic limit, it corresponds to,

$$\frac{U}{Nt} = -\frac{x}{8\frac{JS^2}{t}} - \frac{JS^2}{t}. \tag{9}$$

The energies of each CP3 and CP2 polarons are respectively $-\frac{1}{8\frac{JS^2}{t}} - \frac{2JS^2}{t}$ and $-\frac{1}{8\frac{JS^2}{t}} - \frac{JS^2}{t}$.

Let us mention that homogeneous spiral phases ($\theta_i = \theta$) could be possible ground states. In the thermodynamic limit, these phases can occur for $\frac{JS^2}{t} \geq \frac{\sin \pi x}{2\pi}$ and have energy

$\frac{U}{t} = -\frac{(\sin \pi x)^2}{2\pi^2(\frac{JS^2}{t})} - \frac{JS^2}{t}$. However, our Monte Carlo results show that these are never stable within the model used here. This can be proved analytically in the thermodynamic limit using the expressions we have derived for the different phases, except for the T-phase for which numerical results are necessary. In two-dimension however, renewed interest in a spiral state results from experiments indicating a spin glass behavior of high-T_c $La_{2-x}Sr_xCuO_4$ at small doping [17].

Of course, all the phase separations involving CP3 (AF + CP3, CP3 + P2, CP3 + CP2) present the spin configuration degeneracy (θ_1, θ_2) of the CP3 polarons. This analytical continuous degeneracy is consistent with a spin glass state. Therefore, we propose that the ground state of $Y_{2-x}Ca_xBaNiO_5$ for the studied hole doping $x < 0.15$ [6] belongs to the AF + CP3 phase providing a plausible explanation for the observed spin-glass-like behavior. It is interesting to note that such a possibility of polarons immersed into an anti-ferromagnetic background has been invoked by Xu et al. [18] to fit their neutron data. Finally, we remark that the size chosen for the linear chain $N = 60$ sites and the boundary conditions do not change the nature of the phases involved in the phase diagram.

4. Conclusions

In this work, we presented an unifying picture for the magnetic phase diagram of the one-dimensional DE + SE model using large Hund's coupling and classical localized spins. The solution is in general a) phase separation between F and AF phases for low SE interaction energy and b) phase separation between small polaronic and AF phases when the SE interaction is large. In a large SE limit a Wigner crystallization and a spin-glass behavior can be identified. A spin-glass behavior can be obtained under the condition $\frac{JS^2}{t} \gtrsim \frac{1}{4\sqrt{2}} \approx 0.177$, when CP3 phase exists and could explain the spin-glass-like behavior observed in the nickelate one-dimensional doped compound $Y_{2-x}Ca_xBaNiO_5$. On the other hand, density matrix elements suggest an important lattice distortion in the phases involved in the phase diagram.

Acknowledgments

We want to acknowledge partial support from CONACyT Grant-57929 and PAPIIT-IN108907 from UNAM. E.V. would like also to thank CONACyT and DGAPA-UNAM for financial support.

References

[1] D.C. Mattis, The Theory of Magnetism Made Simple, World Scientific, Singapore, 2006.
[2] P.W. Anderson, H. Hasegawa, Phys. Rev. 100 (1955) 675.
[3] G.H. Jonker, J.H. Van Santen, Physica 16 (1950) 337;
J.H. Van Santen, G.H. Jonker, Physica 16 (1950) 599.
[4] C. Zener, Phys. Rev. 82 (1951) 403;
C. Zener, Phys. Rev. 81 (1951) 440.
[5] P.G. de Gennes, Phys. Rev. 118 (1960) 141.
[6] J.F. DiTusa, et al., Phys. Rev. Lett. 73 (1994) 1857;
K. Kojima, et al., Phys. Rev. Lett. 74 (1995) 3471.
[7] E. Vallejo, M. Avignon, Phys. Rev. Lett. 97 (2006) 217203;
E. Vallejo, M. Avignon, Rev. Mex. Fís. S 53 (7) (2007) 1–6;
E. Vallejo, M. Avignon, J. Magn. Magn. Mater. 310 (2007) 1130.
[8] C.D. Batista, J. Eroles, M. Avignon, B. Alascio, Phys. Rev. B 58 (1998) R14689;
C.D. Batista, J. Eroles, M. Avignon, B. Alascio, Phys. Rev. B 62 (2000) 15047.
[9] D.J. Garcia, et al., Phys. Rev. Lett. 85 (2000) 3720;
D.J. Garcia, et al., Phys. Rev. B 65 (2002) 134444.
[10] W. Koshibae, M. Yamanaka, M. Oshikawa, S. Maekawa, Phys. Rev. Lett. 82 (1999) 2119.
[11] H. Aliaga, et al., Phys. Rev. B 64 (2001) 024422.
[12] S. Yunoki, et al., Phys. Rev. Lett. 80 (1998) 845;
E. Dagotto, et al., Phys. Rev. B 58 (1998) 6414.
[13] D.R. Neuber, et al., Phys. Rev. B 73 (2006) 014401.
[14] S. Yunoki, A. Moreo, Phys. Rev. B 58 (1998) 6403.
[15] M. Yamanaka, W. Koshibae, S. Maekawa, Phys. Rev. Lett. 81 (1998) 5604.
[16] W. Koller, et al., Phys. Rev. B 67 (2003) 174418.
[17] M. Raczkowski, R. Frésard, A.M. Oleś, Europhys. Lett. 76 (2006) 128.
[18] G. Xu, et al., Science, New Series 289 (2000) 419.